Astron. Astrophys. 343, 697–704 (1999)

ASTRONOMY AND ASTROPHYSICS

An analysis of 900 rotation curves of southern sky spiral galaxies: is galaxy evolution constrained to occupy discrete states?

D.F. Roscoe

School of Mathematics, Sheffield University, Sheffield, S3 7RH, UK (D.Roscoe@ac.shef.uk)

Received 17 July 1998 / Accepted 27 October 1998

Abstract. A rudimentary analysis of the 21 rotation curves given by Rubin et al. (1980) based on the hypothesis that $V_{rot} = A\,R^{\alpha}$ where $(\alpha,\ A)$ are constants particular to any given rotation curve, raised the further hypothesis that the distribution of the parameter $\ln A$ (estimated by linear regression on the rotation curves) has a discrete structure which, if representing an underlying real physical effect, would imply that the dynamics of spiral galaxies are constrained to occupy discrete states.

The availability of the very large H_{α} rotation curve data base of spiral galaxies (Persic & Salucci, 1995; PS hereafter) has provided an opportunity to conduct a strong test of this idea, and we find it confirmed at a level of almost certainty on the data analysed. Given the already well known strong relationship between rotational kinematics and luminosity properties of galaxies, this result implies that the luminosity evolution of spiral galaxies is constrained to occur on discretely defined surfaces so that, finally, a form of 'cosmic coherence' for galaxy evolution appears to be suggested.

Key words: galaxies: fundamental parameters – galaxies: kinematics and dynamics – galaxies: spiral – cosmology: dark matter

1. Introduction

The hypothesis to be tested is based, primarily on the assumption that the power-law structure, $V_{rot} = A\,R^{\alpha}$, provides an appropriate formalism for the modelling of the kinematics within optical discs. The fitness of this formalism for the purpose has been exhaustively investigated and very strongly confirmed in Roscoe (1999). The basic conclusion reached there is that, at the very least, the power-law model represents an extremely good approximation to the idealized reality (that is, in the absence of the inevitable disc irregularities) once the effects of the bulge on optical-disc dynamics have been properly accounted for. The data-reduction process by which this latter objective was achieved is described in Roscoe and, briefly, it amounts to a *prior-decided* means of minimizing the effect of the bulge on the rotation-curve calculations, and is assumed to be an integral part of the analysis presented here.

Send offprint requests to: D.F. Roscoe

The particular hypothesis to be tested *in the first instance* arose from a simple analysis of the 21 rotation curves of late-type spirals given by Rubin et al. (1980), hereafter RFT, and is that when the phenomenological power-law model, given by

$$V_{rot} = A\left(\frac{R}{R_0}\right)^{\alpha}, \tag{1}$$

is fitted to optical rotation curve data of, specifically, late-type spiral galaxies then there exists a scaling factor, R_0, somewhere in the range $(0.5, 1.0)\,kpc$ which is such that the distribution of the corresponding $\ln A$ is periodic with period of 0.5 and with a zero phase. The following analysis finds a positive result on PS data for the scaling $R_0 \approx 1/1.7$, and estimates the significance of the result via an extensive Monte-Carlo simulation which consisted of 2×10^6 trial analyses of synthetic data; the conclusion of this initial analysis was that the hypothesis is supported on PS data for late-type spirals at a confidence level of 99.994% - equivalent to about a 1:16000 chance. However, the analysis found no evidence at all to support the extension of the hypothesis to the case of early-type spirals.

Before considering the discrepancy between a positive result for late-type spirals and a negative result for early-type spirals, it is necessary to understand the purpose for which the numerical scaling factor, R_0, was introduced into (1): RFT defined their galactic linear scales on the basis of Hubble distances which were estimated using $H = 50\,km/sec/mpc$. This latter figure is now known to be too small by a considerable margin, so that the RFT galactic linear scales are too big by a corresponding factor. The introduction of the R_0 scaling factor can therefore be seen as a device designed to rescale Tully-Fisher derived galactic linear scales in the PS data so that they approximated RFT's Hubble-derived galactic linear scales. By this process, it then became possible to test a hypothesis raised on the RFT data directly against PS data.

Once the scaling factor, R_0, is recognized as merely a computational device designed to compensate for a biased parameter estimate (that of $H = 50\,\mathrm{km/sec/mpc}$), then we have a rationale for reconsidering the data in its Tully-Fisher (TF hereafter) scaled form (that is, effectively using $R_0 = 1$). When this was done, it was found that the $\ln A$ peaks, found to exist with a half-integer, zero-phase periodicity in the Hubble-scaled data ($R_0 = 1/1.7$) for late-type spirals, were shifted to differ-

ent positions in the TF-scaled data. But now, it was found that these peaks in late-type spiral data coincided *exactly* with similar peaks in early-type spiral data - a coincidence which did not exist in the Hubble-scaled data ($R_0 = 1/1.7$) because of the non-linear nature of the transform of $\ln A$ under the rescaling process (see Appendix B).

So, to summarize, a simple analysis of late-type spiral data given by RFT led to the hypothesis that, for an appropriate linear scaling, $\ln A$ data has a half-integer, zero-phase periodicity; this hypothesis was confirmed, via extensive Monte-Carlo simulations, at the level of about a 1:16000 chance on Hubble-scaled $\ln A$ data derived from the PS late-type spirals. The existence of this effect was then traced directly to the existence of very strong peaks in the TF-scaled $\ln A$ data for the late-type spirals, and these peaks were then found to be *exactly* mirrored in the TF-scaled $\ln A$ data for early-type spirals.

A conservative estimate of the probability of obtaining the results of this latter analysis by chance, given the original hypothesis raised on RFT data, is about 10^{-7}; We concluded that the effect is confirmed at a level of almost certainty. However, given the profound nature of the result, caution dictates that the analysis is repeated on a similarly sized new data base.

2. The hypothesis and RFT data

The hypothesis arose in the following way: prior to the analysis of Roscoe, the power-law model was preliminarily tested against data drawn from a sample of 21 rotation curves of late-type spirals given in the classical paper of RFT. This testing took the form of performing a linear regression of $\ln V_{rot}$ on $\ln R$ for that subset of twelve rotation curves which manifested purely *monotonic* behaviour, and then recording the regression constants. No scaling factor was introduced for this exercise (equivalent to the the assumption $R_0 = 1.0$.) RFT assumed $H = 50\,\mathrm{km/sec/mpc}$ and used redshifts corrected for the motion of the local group to define Hubble distances; their linear scales were based upon these distance estimates. The results, quoted to two significant figures, are condensed in Table 1. For present purposes, the most striking feature to be observed in this table is that, after taking into account the numerical rounding process, $\ln A$ only takes values which lie within ± 0.15 of an integer or half-integer. The argument to determine the likelihood of this result goes as follows: the probability that a single number, chosen at random from the real line, will lie within ± 0.15 of an integer or half-integer is exactly 0.6. It follows that the probability of every one of a sample of twelve numbers, chosen on the basis of some independent prior criterion, lying within ± 0.15 of an integer or half-integer is $0.6^{12} \approx 0.002$. That is, the RFT data appears to suggest that $\ln A$ might be periodic with period 0.5 and zero phase.

Considering the matter in more detail, we recall that, although RFT used $H = 50\,\mathrm{km/sec/mpc}$ to set their linear scales, the more recent consensus is that $H > 50\,\mathrm{km/sec/mpc}$ by a considerable margin. For example, if $H \approx 70\,\mathrm{km/sec/mpc}$ is accepted as more reasonable than the value applied by RFT, then the linear scales used by them are too great by a factor of 1.4, and such an error has the same *numerical* effect as defining the scaling factor $R_0 = 1/1.4\,kpc$ in (1). In other words, although we notionally set $R_0 = 1.0\,kpc$ in our simple analysis of RFT data, the data reduction process of RFT has implicitly introduced the prior value $R_0 \approx 1/1.4\,kpc$, if it is assumed that $H \approx 70\,\mathrm{km/sec/mpc}$.

Table 1. $V = A\,R^{\alpha}$

Galaxy	Ln(A)	Galaxy	Ln(A)
N3672	3.6	U3691	3.6
N3495	4.0	N4605	4.0
I0467	4.1	N0701	4.1
N1035	4.1	N4062	4.5
N2742	4.5	N4682	4.5
N7541	4.6	N4321	4.9

Given that the RFT data suggests the existence of an $\ln A$ periodicity of 0.5 for the choice of scaling factor $R_0 \approx 1/1.4\,kpc$, we are led to the hypothesis that, for the generality of late-type spiral rotation curve data (the kind considered by RFT), there is a scaling factor, R_0, somewhere in the range defined by $1.0 \leq R_0^{-1} \leq 2.0$ which is such that $\ln A$ is distributed periodically, with period 0.5 and zero phase. This hypothesis is tested against PS data in the following, and an objective assessment of the significance of the obtained result is derived through an extensive Monte-Carlo simulation which consisted of 2×10^6 trial analyses of synthetic data. The final conclusion is that this hypothesis is supported on PS data *for late-type spirals* at a confidence level of 99.994%.

3. The methodology

The most recent determinations of the Hubble constant place it in the range $65 \leq H \leq 75\,\mathrm{km/sec/mpc}$; consequently, since RFT used $50\,\mathrm{km/sec/mpc}$ then, effectively, they introduced a scaling factor defined by $R_0^{-1} \approx 1.4$. Given this, it was considered reasonable to suppose that, if the periodicity effect in $\ln A$ reflects a real physical phenomenon, then the appropriate scaling factor will lie somewhere in the range defined by $1.0 \leq R_0^{-1} \leq 2.0$. Our methodology is designed around this supposition.

In practice, therefore, our analysis introduces eleven experimental scaling factors defined by $R_0^{-1} = 1.0, 1.1, ...2.0$. At each of these scalings, the specific question posed was *how many of the* $\ln A$ *values lie within* ± 0.15 *of either an integer or half-integer value?*

4. The search and results

As we have mentioned, the search process involved introducing eleven experimental scalings defined by $R_0^{-1} = 1.0, 1.1, ..., 2.0$, and then asking the specific question at each rescaling *how many of the* $\ln A$ *values in the given sample lie within* ± 0.15 *of either an integer or half-integer value?* Because these ranges cover 60% of the real line, they are referred

Table 2.

Galaxy Types	Optimal R_0 kpc	Sample Size	Number Of Hits	Single Trial Probability
0..9	1/1.7	900	588	0.561×10^{-3}
0..5	1/1.5	485	304	0.123
6..9	1/1.7	415	292	0.731×10^{-5}

to as 60% bins in the following. The results of the analysis are condensed into Table 2 which shows the results for the optimal rescalings to be used for three partitions of the data. In this table a 'Hit' is defined to be when a particular $\ln A$ lies within one of the 60% bins. The first row considers all the galaxies together, the second row considers early and intermediate types together, whilst the third row considers the late types together; these latter types were the exclusive types of the RFT study. The final column of this table gives the probability of the relevant result occurring by chance alone *assuming that the optimal scaling was chosen correctly without searching*. It is clear from the table that the only significant result occurred for the late-type spirals with a scaling parameter $R_0 = 1/1.7$; however, given that, in practice, a search over a range of eleven (adjacent) experimental scalings was executed then the actual probabilities are at least an order of magnitude less significant. These actual probabilities were assessed using Monte-Carlo simulations, as briefly described in the following section.

5. A Monte-Carlo simulation

The only really significant result arising from the scale-search process was that associated with the late-type spirals. However, the adjacent nature of successive experimental rescalings means that each experiment is not strictly independent of its neighbours, and it therefore becomes difficult to assess the probability of the obtained result (292 hits out of a sample of 415 type 6..9 spiral galaxies) accurately. This problem was resolved using Monte-Carlo simulations, the details of which are described extensively in Appendix A, and the probability of obtaining the result of Table 2 was computed at 6.2×10^{-5} (about a 1:16000 chance) over 2×10^6 simulations.

6. The TF-scaled Ln(A) data for late-type spirals

As we have mentioned, the introduction of the numerical scaling factor, $R_0 = 1/1.7$, in (1) was essentially a device whose effect was to make TF-scaled $\ln A$ data transform approximately into Hubble-scaled $\ln A$ data with $H = 50\,\mathrm{km/sec/mpc}$ so that, finally, a hypothesis raised on RFT data could be tested directly using PS data. For the remainder of this paper, we reconsider the data in its natural TF-scaling, and refer to $\ln A$ data scaled using $R_0 = 1/1.7$ as 'Hubble-scaled data'. The first requirement is to understand the relationship between TF-scaled $\ln A$ data and the Hubble-scaled $\ln A$ data.

Table 3. $\ln A$ Data

Hubble Scaling	TF Scaling
2.5	2.99
3.0	3.40
3.5	3.81
4.0	4.22
4.5	4.63
5.0	5.04
5.5	5.45

Referring to the Hubble-scaled $\ln A$ data as $\ln A_{1/1.7}$ and the TF-scaled $\ln A$ data as $\ln A_{1.0}$, we show, in Appendix B, that $\ln A_{1/1.7}$ and $\ln A_{1.0}$ are related by

$$\ln A_{1.0} \approx 0.82 \ln A_{1/1.7} + 0.94. \quad (2)$$

It follows that, using this relationship, we can estimate how integer/half-integer values of $\ln A$ in the Hubble-scaled data transform into TF-scaled $\ln A$ values.

We make use of this information in the following way: Considering the Hubble-scaled data ($R_0 = 1/1.7$), we firstly isolate those late-type rotation curves for which $\ln A$ lies within ± 0.1 of an integer or half-integer and then, for this subset of rotation curves, calculated $\ln A$ using the TF-scaling ($R_0 = 1.0$). The Hubble-scaled and TF-scaled $\ln A$ data are then plotted adjacently in Fig. 1, where the Hubble-scaled data is shown in the upper diagram. It is clear that the TF-scaled $\ln A$ data is considerably shifted with respect to the Hubble-scaled data so that the exact correlation between the two sets of data is not clear. To clarify this correlation we use (2) above to estimate the values of $\ln A_{1.0}$ corresponding to $\ln A_{1/1.7} = 2.5, 3.0, 3.5, 4.0, 4.5, 5.0, 5.5$. The correspondence between Hubble-scaled and TF-scaled $\ln A$ values is given in Table 3, and the tabulated TF-scaled $\ln A$ values are indicated as vertical dotted lines in the lower part of Fig. 1. These dotted lines allow us to make the correct associations between the Hubble-scaled and the TF-scaled data, and these associations are indicated by the labelling A0, A, B, C, D, E and F. We see that peak A0 in the Hubble-scaled data has completely lost its fidelity in the transformation to the TF-scaling (reference to Appendix B shows that (2) depends on α-data, so that this loss of fidelity is probably due to the large scatter in α-data for low $\ln A$ apparent in Fig. A1 of Appendix A). By contrast, peak A in the Hubble-scaled data has retained reasonable fidelity in its transformation to the TF-scaling, whilst peaks B, C, D, E and F have transformed with improved fidelity into the TF-scaling.

Finally, in Fig. 2, we show the complete set of TF-scaled $\ln A$ data for late-type spirals in the upper diagram and, in the lower diagram, we reproduce the lower diagram of Fig. 1. However, the dotted lines now represent the centre-lines of the peak-maxima of the lower diagram, and it can be seen that these also coincide with the peak-maxima of the upper diagram. Remembering that the lower diagram represents the transformation of the integer/half-integer peaks in Hubble-scaled $\ln A$ data to the

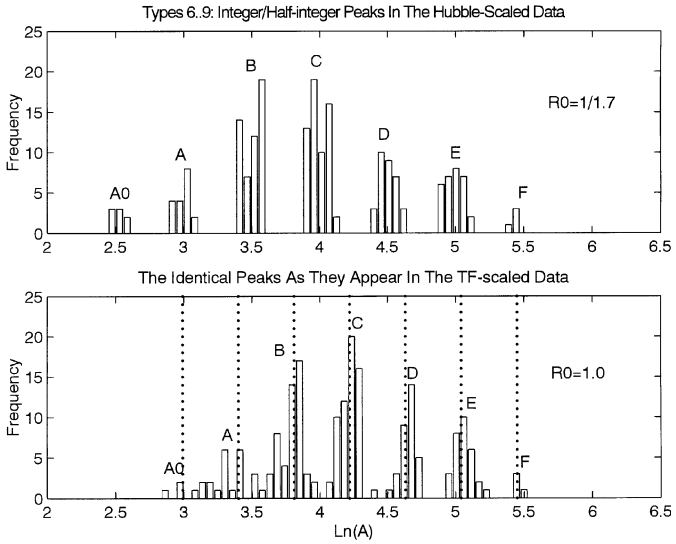

Fig. 1. Transformation of Hubble-Scaled $\ln A$ peaks to TF-scaling

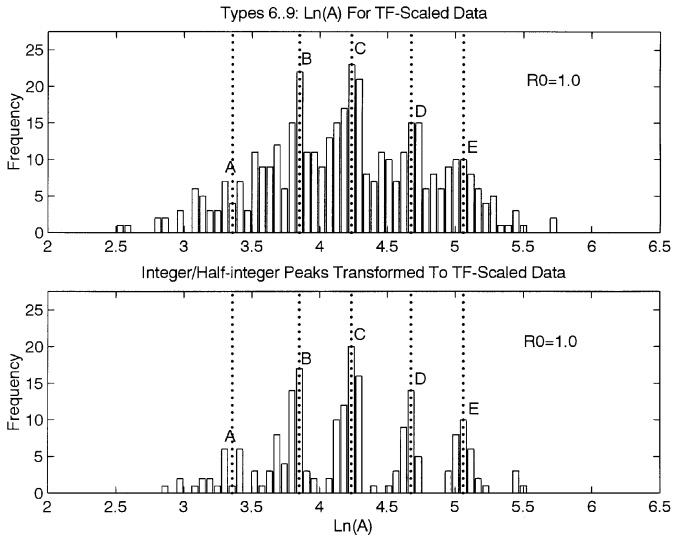

Fig. 2. Identity between TF-scaled and Hubble-scaled $\ln A$ peaks

TF-scaling, then the dotted lines of Fig. 2 make it clear that the integer/half-integer peaks of Hubble-scaled $\ln A$ data (as represented in the TF-scaled lower diagram) correspond exactly to true peaks in the TF-scaled $\ln A$ data, represented in the upper diagram. In other words, the peaks A, B, C, D and E of the upper diagram in Fig. 2 correspond exactly to the 3.0, 3.5, 4.0, 4.5 and 5.0 peaks originally hypothesised to exist on the basis of the RFT data. The remaining peaks, A0 and F (not indicated in Fig. 2), are too small to be separated reliably from the noise.

7. The TF-scaled Ln(A) data for early-type spirals

In this section, we show that the TF-scaled $\ln A$-data for early-type spirals has virtually the same peak-structure as the TF-scaled $\ln A$-data for the late-type spirals.

The upper diagram of Fig. 3 shows TF-scaled $\ln A$ data for the early-type spirals whilst the lower diagram, which reproduces the lower diagram of Fig. 2, shows the already identified peaks in the TF-scaled $\ln A$ data for the late-type spirals with the centres of the peak-maxima being indicated by the vertical dotted lines. It is clear that the major late-type peaks B, C and E (lower diagram) have exact matches in the early-type data (upper diagram) whilst peak D in the late-type data has a reasonably close match on the early-type data. The peaks A0 and F cannot be separated from the noise in the early-type data whilst there is an indication that peak A in late-type data is reflected in the early-type data.

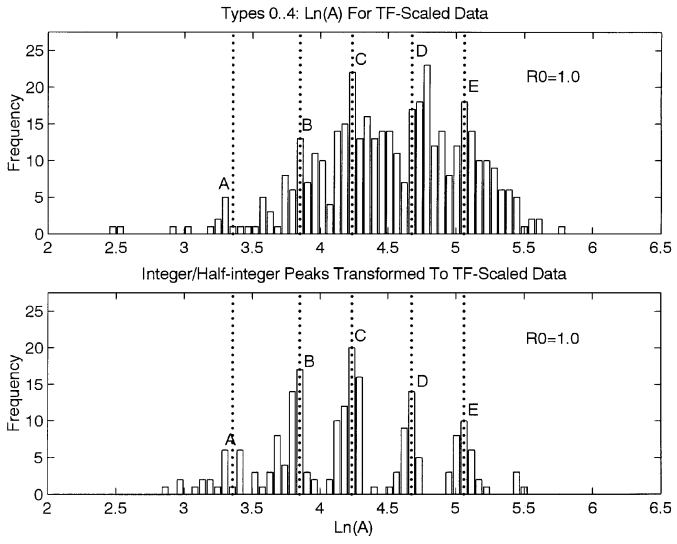

Fig. 3. Correspondence between early-type and late-type $\ln A$ data

Since Fig. 3 makes it plain that the peak-structure of TF-scaled $\ln A$ data for late-type spirals is reflected in the peak-structure of TF-scaled $\ln A$ data for early-type spirals, it becomes natural to ask why the Hubble-scaled $\ln A$ data for early-type spirals fails to show the half-integer periodicity which was manifest on the Hubble-scaled $\ln A$ data for late-type spirals. This question is considered in detail in Sect. 9

8. The TF-scaled Ln(A) data for the complete data set

In the previous section, we have shown how the peaks B, C, and E in TF-scaled $\ln A$ data for late-type spirals appear to have their exact counterparts in the corresponding data for early-type spirals, whilst peak D of early-type data has a reasonably close late-type counterpart.

In this section, the TF-scaled $\ln A$ data for all 900 rotation curves in the data base is combined and shown in Fig. 4; the vertical dotted lines in the figure indicate the positions of peak-maxima in the $\ln A$ data for the specifically *late-type* spirals, and are therefore identical to those shown in Fig. 2. It is clear from Fig. 4 that the peaks A, B, C, D and E in the late-type data have been dramatically boosted by the corresponding peaks in the early-type data; in fact, it is now the case that all four of the peaks B, C, D and E in the combined sample coincide exactly with the corresponding peaks in the specifically late-type data. In addition to this, it becomes clear that peak A, identified in Fig. 1,

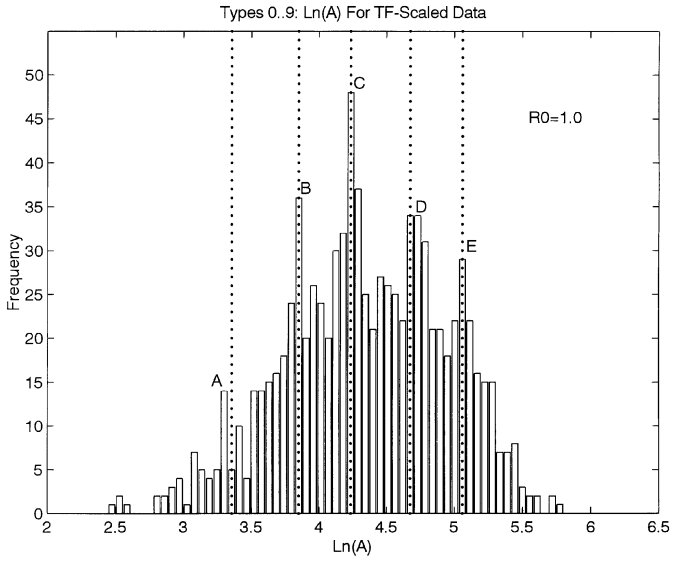

Fig. 4. Magnification of identified peaks in 900 rotation curves

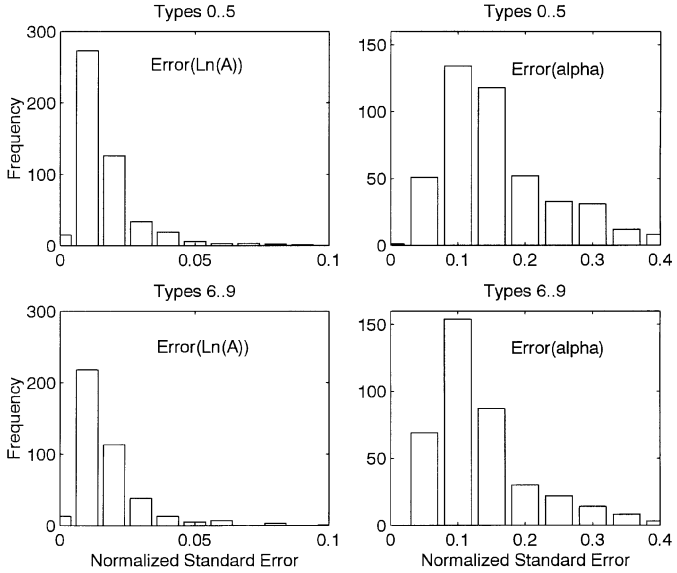

Fig. 5. Normalized standard errors in $\ln A$ data and α data

but partly discounted in Figs. 2 and 3 because of background noise, is significantly enhanced in Fig. 4.

In summary, it is very clear that the effect of combining the early-type data with late-type data has been to magnify the peaks A, B, C, D and E very considerably above the background noise. This magnifying effect makes it possible to reach the strong conclusion that the peak-structure in $\ln A$ data for late-type spirals, which was effectively hypothesised to exist on the basis on the RFT data, also exists on $\ln A$ data for early-type spirals.

9. A qualitative error analysis

We showed, in Sect. 7 and Sect. 8, that TF-scaled $\ln A$ data for early-type spirals has the same peak structure as the corresponding data for late-type spirals. Given this, it becomes natural to consider why the Hubble-scaled $\ln A$ data for early-type spirals failed to exhibit the half-integer periodicity exhibited by the corresponding data for late-type spirals. We show that the probable reason for the discrepancy lies in the dual circumstances:

1. the transformation to Hubble-scaled $\ln A$ data from the TF-scaled $\ln A$ data involves α data through (A2) of Appendix A;
2. the observation that the α data for early-type spirals turns out to be considerably noisier than the corresponding data for late-type spirals.

These two circumstances together mean that Hubble-scaled $\ln A$ data is more accurately defined for late-type spirals than it is for early-type spirals, and this is consistent with the fact that peaks which are seen in TF-scaled $\ln A$ data for both early and late-type spirals only have detectable counterparts in the Hubble-scaled data of the late-type spirals.

As a means of investigating the possibilities, we consider the normalized standard regression errors (that is, [standard error]/[expected value]) of the parameters $(\alpha, \ln A)$ in each galaxy class, and their distributions are shown in Fig. 5. The distributions for $\ln A$ data are shown in the two left-hand diagrams, and it is clear that the distributions are very similar. By contrast, the distributions for α data, shown in the two right-hand diagrams, are markedly different in the sense that the proportion of α-values with a normalized standard error > 0.1 is very much higher in the early-type data than in the late-type data.

It follows from this simple analysis that the TF-scaled $\ln A$-data possesses similar accuracy for both early and late-type spirals, whilst the Hubble-scaled $\ln A$ data - which depends on α-data - will be more accurately defined for the late-type spirals than for the early-type spirals. These findings are consistent with the failure to detect integer/half-integer periodicity in the Hubble-scaled $\ln A$ data for early-type spirals.

10. Discrete structure in α-data

Since, as Fig. A1 in Appendix A makes very plain, $\ln A$ and α are very strongly correlated, and since we have shown that $\ln A$ data appears to have a discrete structure, then it might be expected that α should manifest a similarly discrete structure. However, detailed investigations have failed completely to identify any such structure, and Fig. 6 shows why - even if the hypothesised structure really does exist.

The upper diagram shows the distribution of the normalized standard regression errors of $\ln A$ data, whilst the lower diagram shows the distribution of the normalized standard regression errors of α data drawn on the same scale. It is clear that the normalized standard regression errors for α data are about five times greater than the corresponding errors for the $\ln A$ data, with a mean of about 0.1. Given that five peaks, A, B, C, D and E have been identified in $\ln A$ data in the range $3 \leq \ln A \leq 5.5$, then, as reference to Fig. A1 makes plain, we should expect also five peaks in α data in the range $0 \leq \alpha \leq 1.0$ - so that the peaks would be expected to have a mean separation of about

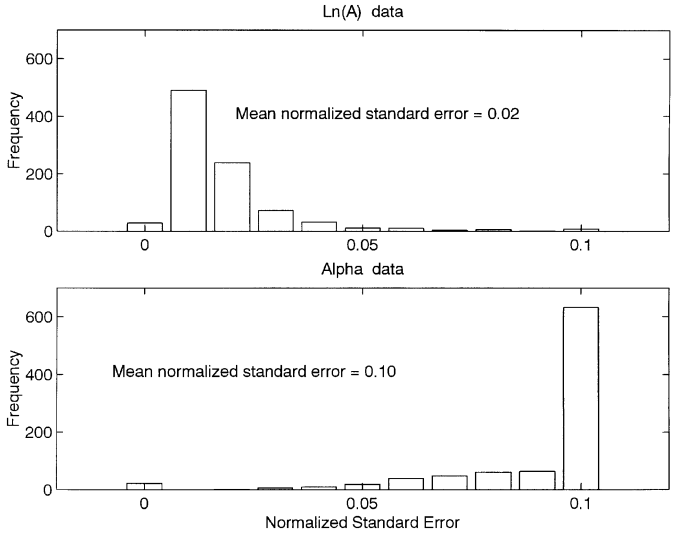

Fig. 6. Comparison of normalized standard errors between $\ln A$ and α data

0.2. However, the mean normalized standard error of α data of about 0.1 is entirely sufficient to destroy any signal in α data with a mean period of about 0.2.

11. Assessment of probability

The original hypothesis, raised on RFT data, was confirmed in the late-type spiral PS data with a probability of about 6×10^{-5} (obtained from extensive Monte-Carlo simulation) of it being a chance effect. Since the labelled peaks in the upper diagram of Fig. 2 represent the TF-scaled evidence supporting this hypothesis for late-type spirals, then the above mentioned probability of 6×10^{-5} can be associated with this diagram. The objective now is to attempt an assessment of the probability that the major peaks, B, C, D and E, of Fig. 4, have arisen at exactly the positions of the corresponding peaks in Fig. 2 by chance alone.

The peaks B, C, D and E of Fig. 4 are as dominant as they are because the corresponding peaks in the upper diagram of Fig. 2 have been boosted in exactly the right way by the data represented in the upper diagram of Fig. 3, which refers to early-type spirals. Of the peaks B, C, D and E in Fig. 3, three of them (B, C and E) occur at exactly the same histogram bar as the corresponding peaks in Fig. 2; the fourth, D, provides a close match. Suppose we discount the close match of D, and consider only the probability of coincidence between peaks B, C and E. In the range $3.5 \leq \ln A \leq 5.5$, there are 36 histogram bars (each is of width 0.055), and so the question is equivalent to asking the probability of picking three red bricks out of a box containing 32 black bricks and four red bricks in four trials, and with no replacements. Since the probability of this happening is about 2×10^{-3}, then the overall probability of Fig. 2 and Fig. 3 occurring as they do, given the original hypothesis raised on RFT data, is about $(6 \times 10^{-5}) \times (2 \times 10^{-3}) \approx 10^{-7}$, or about 1:10,000,000.

This level of probability suggests very strongly that the hypothesised phenomenon reflects a fundamental physical reality; however, the implications for our understanding of galactic evolution are so profound, that extreme caution is indicated as an appropriate response - specifically, the subject requires, at the very least, a second analysis of a similarly sized independent data-base.

12. Discussion

The foregoing analysis has shown that a hypothesis, originally raised on RFT rotation curve data, for discrete structure in the distribution of $\ln A$, is confirmed on PS data at an extremely high level of confidence. Always bearing in mind that such a profound claim requires the highest level of substantiation, it is worthwhile discussing the implications of the presented results. To aid the discussion, we make the working assumption that, if $\ln A$ has discrete structure, then so also does α.

According to the analysis of Roscoe, the rotational kinematics and luminosity properties of spiral galaxies are very strongly connected through the relationship

$$\begin{aligned} \log A &= \log V_0 - \alpha \log R_0, \text{ where} \\ \log V_0 &\approx -0.584\text{–}0.133\, M - 0.000243\, S, \\ \log R_0 &\approx -3.291\text{–}0.208\, M - 0.00292\, S, \end{aligned} \tag{3}$$

where M represents absolute magnitude and S represents surface brightness. Note that this latter relationship uses base-10 logarithms, rather than natural logarithms. Consequently, if $\ln A$ and α have discrete structure, then M and S are constrained by the above relationship to lie in any one of a set of discretely defined surfaces. Thus, the basic discreteness would lie, not in the kinematics, but rather in the idea that the luminosity evolution of spiral galaxies would be constrained to occupy discrete state planes.

Given this, there are then two possibilities: either a galaxy is 'born' on a given state plane, and then simply exhibits evolving luminosity properties over its whole life remaining on that plane; or the process of galactic evolution involves very rapid transitions between state planes which punctuate long periods of equilibrium occupying a single state plane.

The theoretical difficulty raised by both of these interpretations concerns the implication of a cosmic coherence, whereby any given state plane at any given time is a shared state of some large subclass of all spirals.

13. Conclusions

Beginning with an hypothesis originally raised on RFT optical rotation curve data, we have shown that when $V_{rot} = A\, R^{\alpha}$ is fitted to the data, and after the effects of the bulge on the optical disc have been accounted for, then $\ln A$ appears to have a preference for certain discrete values. When linear scales are defined on the basis of Tully-Fisher distance estimates, these preferred values are those listed in Table 4; the probability of this being a chance effect has been conservatively estimated at about

Table 4. Predicted positions of major Ln(A) peaks

3.36	3.85	4.24	4.68	5.06

10^{-7}. Even though the probabilities associated with this study are vanishingly small, its implications for our understanding of galactic evolution are so profound that, at a minimum, at least one other similar study of independent data should be made.

Appendix A: the Monte-Carlo simulation

The requirement was to perform 2×10^6 simulations, each of them effectively repeating the calculation of Sect. 4 on synthetic data.

The direct approach would have been to generate 2×10^6 sets of synthetic (R, V_{rot}) data (each consisting of 900 synthetic rotation curves) from the real data, and then to repeat the whole process as so far described for each such synthetic set. However, such an approach would be extremely costly in its computing requirements, and a very much more efficient approach exists as described in the following.

Introduce the notation

$$V_{rot} = A_{R_0} \left(\frac{R}{R_0} \right)^{\alpha},$$

so that the constant A_{R_0} corresponds to the scaling, R_0. From this latter relationship we have, for arbitrary R_0, and for the specific case $R_0 = 1$, the respective relationships

$$\begin{aligned} \ln V_{rot} &= \ln A_{R_0} - \alpha \ln R_0 + \alpha \ln R \qquad \text{(A1)} \\ \ln V_{rot} &= \ln A_1 + \alpha \ln R, \end{aligned}$$

from which it follows immediately that

$$\ln A_{R_0} = \ln A_1 + \alpha \ln R_0. \qquad \text{(A2)}$$

Consequently, if $\ln A_1$ and α are calculated for any given rotation curve through linear regression on (R, V_{rot}) data with $R_0 = 1$, then the corresponding value of $\ln A_{R_0}$, for an arbitrary $R_0 \neq 1$, can be efficiently computed using (A2).

A direct implication of this simple result is that we can work directly with the real $(\alpha, \ln A)$ data generated just once for the case $R_0 = 1$ on the real rotation curve data, and subsequently use this to generate synthetic $(\alpha, \ln A)$ data corresponding to a synthetic $R_0 = 1$ case. Once we have such an $R_0 = 1$ synthetic data set, the computations of $\ln A_{R_0}$ for $R_0 \neq 1$ synthetic data can be efficiently completed using (A2).

A.1. formation of synthetic data sets

Although we are primarily interested in the distribution of $\ln A$ across the sample of rotation curves, (A2) shows that an efficient recomputation of $\ln A_{R_0}$ at each experimental rescaling requires knowledge of the α distribution as well. Correspondingly, the task is to generate synthetic distributions of $(\alpha, \ln A)$, rather than solely $\ln A$, from the real data. The process is described in the following algorithm.

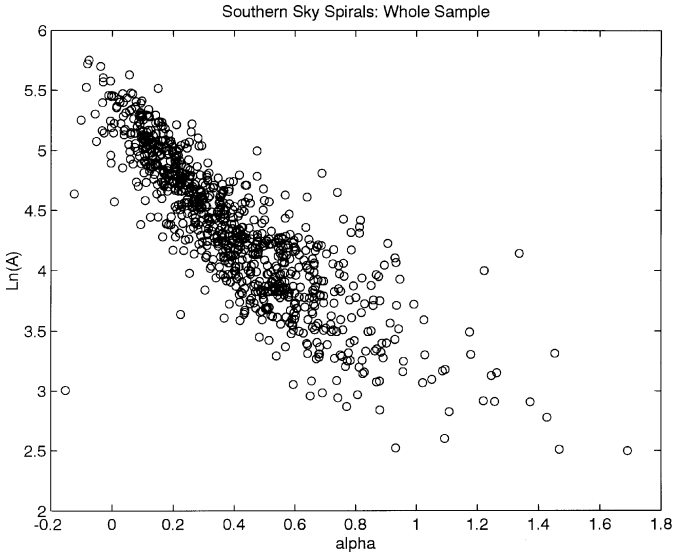

Fig. A1. $(\alpha, \ln A)$ plotted for each of 900 rotation curves

- Randomly select five $(\alpha, \ln A)$ pairs from that list of 415 such pairs which correspond to late-type spirals and label them as $(\alpha_1, \ln A_1)...(\alpha_5, \ln A_5)$;
- Generate five random numbers, $p_1...p_5$ on the range $(0, 1)$;
- Form synthetic values, $(\alpha, \ln A)$, as weighted averages according to

$$\begin{aligned} \alpha &= \frac{p_1\alpha_1 + .. + p_5\alpha_5}{p_1 + .. + p_5} \\ \ln A &= \frac{p_1 \ln A_1 + .. + p_5 \ln A_5}{p_1 + .. + p_5}. \end{aligned}$$

- Repeat the whole process 415 times to generate a synthetic data set of equal size to the real data set.

Whilst this process creates a synthetic distribution from the real distribution in a way which preserves that distribution's mean values and its overall shape (the envelope of the synthetic distribution is geometrically similar to that of the real distribution) it cannot preserve variance in the distribution. This is because the adopted process creates a new distribution which is squeezed *inside* the boundaries of the original distribution. This is easily understood by considering an identical process performed on a one-dimensional distribution of numbers; in this latter case, the synthetic distribution is easily seen to be necessarily contained *within* the original distribution. Consequently, the process of generating a synthetic distribution is completed by expanding the distribution obtained at the first stage in a self-similar way about its median point until the extremities of its envelope match those of the real distribution. The real $(\alpha, \ln A)$ distribution, plotted for $R_0 = 1$, is shown in Fig. A1, whilst a typical synthetic distribution derived from this real data is shown in Fig. A2.

A.2. the simulation process

The problem is to obtain an objective assessment of the significance of the 292 hits out of 415 trials recorded for late-type

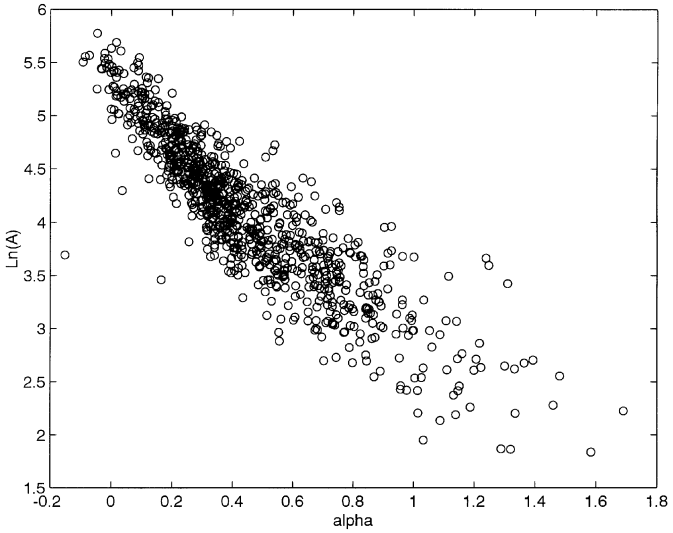

Fig. A2. Typical synthetic $(\alpha, \ln A)$ data

spirals in Table 2, and the Monte-Carlo process constructed to arrive at this assessment consisted of 2×10^6 individual simulations, each one of which has the following structure:

The real data consists of the 415 pairs of $(\alpha, \ln A)$ values computed by linear regression on the basic PS data using a scaling factor of $R_0 = 1$, and is therefore denoted as $(\alpha, \ln A_1)$ data. Each individual simulation uses this real data to generate 415 sets of synthetic $(\alpha, \ln A_1)$ data. At each simulation, eleven experimental scalings, defined by $R_0^{-1} = 1.0, 1.1, ..., 2.0$, were introduced and, for each such length scale, the synthetic $(\alpha, \ln A_1)$ data was used to generate synthetic $(\alpha, \ln A_{R_0})$ data using (A2). At each such experiment, the specific question was then asked *how many of the 415 synthetic* $\ln A_{R_0}$ *values lies within* ± 0.15 *of an integer or half-integer?* If the answer to this latter question was 292 or more 'hits' then a record was kept; otherwise no record was kept.

After 2×10^6 such simulations it was found that only 124 of them recorded 292 or more hits out of the 415 trials involved in each simulation. Consequently, the probability of the results of Table 2 arising purely by chance was assessed at 6.2×10^{-5}, which is equivalent to a confidence level of 99.994%

Appendix B: the transformation between Hubble-scaled and TF-scaled Ln(A) data

Eq. (A2) of Appendix A gives, for $R_0 = 1/1.7$,

$$\ln A_{1.0} = \ln A_{1/1.7} + 0.53\,\alpha, \tag{B1}$$

where $\ln A_{1.0}$ refers to the value of $\ln A$ in the TF-scaled data, and $\ln A_{1/1.7}$ refers to its value in the Hubble-scaled data.

Furthermore, it is clear from Fig. A1 that $\ln A_{1.0} \approx a_0 + b_0\,\alpha$ for some $(a_0,\, b_0)$; in principle, therefore, α can be eliminated from (B1) in favour of $\ln A_{1.0}$ to give an equation relating $\ln A_{1.0}$ directly to $\ln A_{1/1.7}$. Various estimates for the approximation $\ln A_{1.0} \approx a_0 + b_0\,\alpha$ are given in Roscoe at Table 3 all of which suit the present purpose. One particular estimate, obtained by a minimization procedure, is give as

$$\ln A_{1.0} \approx 5.27\text{–}2.44\,\alpha,$$

and this, when substituted into (B1), gives

$$\ln A_{1.0} = 0.82\,\ln A_{1/1.7} + 0.94.$$

References

Mathewson D.S., Ford V.L., Buchhorn M., 1992, ApJS 81, 413
Nelder J.A., Mead R., 1965, Comp. J. 7, 308
Persic M., Salucci P., 1995, ApJS 99, 501 (=PS)
Roscoe D., 1999, A&A 343, 697
Rubin V.C., Ford W.K., Thonnard N., 1980, ApJ 238, 471 (=RFT)